5-2-2018

Photoinduced interfacial charge separation dynamics in zeolitic imidazolate framework

Brian Pattengale
Marquette University

Jier Huang
Marquette University, jier.huang@marquette.edu

Chemistry Faculty Research and Publications/College of Arts and Sciences

Photoinduced interfacial charge separation dynamics in zeolitic imidazolate framework

Brian Pattengale: Department of Chemistry, Marquette University, Milwaukee, Wisconsin
Jier Huang: Department of Chemistry, Marquette University, Milwaukee, Wisconsin

Abstract

Owing to their porous structure and tunable framework, zeolitic imidazolate frameworks (ZIFs) have garnered considerable attention as promising photocatalytic materials. However, little is known regarding their photophysical properties. In this work, we report the photoinduced charge separation dynamics in a ZIF-67 thin film through interfacial electron transfer (ET) to methylene blue (MB^+) via ultrafast transient absorption spectroscopy. We show that the ET process occurs through two distinct pathways, including an ultrafast (<200 fs) process from the $[Co^{II}(mim)_2]$ units located on the surface of ZIF-67 film that are directly in contact with MB^+ and a relatively slower ET process with a 101.4 ps time constant from the units in the bulk of the film that were isolated from MB^+ by the surface units. This first direct evidence of the ET process from ZIF-67 to electron acceptor strongly suggests that ZIF materials may be used as intrinsic photocatalytic materials rather than inert hosts.
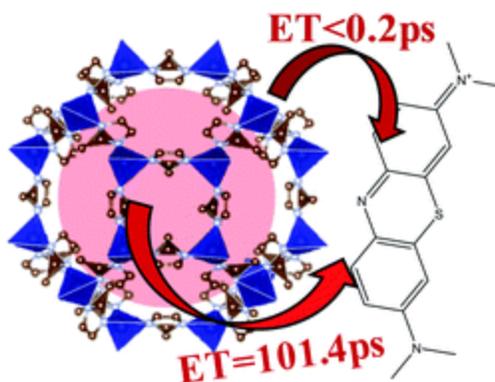
Introduction

Zeolitic imidazolate frameworks (ZIFs) are a subclass of metal–organic frameworks (MOFs) that are composed of primarily Co^{II} or Zn^{II} metal nodes tetrahedrally coordinated by imidazolate linkers.[1–3] In addition to sharing the same topology with zeolites, ZIFs exhibit excellent thermal and chemical stability.[4,5] However, ZIFs are particularly advantageous over traditional zeolite materials in their structural flexibility due to the diversity of imidazolate ligands available,[5,6] and the ability to dope metals[1,7–10] or different mixtures of ligands[11,12] into the framework. These characteristics, together with their inherently large surface areas and high porosity, make ZIFs ideal materials for catalytic applications. Indeed, recent studies have demonstrated ZIFs' catalytic activity in diverse reactions such as the Friedel–Crafts acylation,[13] the Knoevenagel reaction,[14] alkene hydrogenation etc.[15] Very recently, ZIFs have also been used in photocatalysis including dye[16] and phenol[17] degradation as well as CO_2 reduction[18,19] and H_2 generation[20,21] in the presence of molecular photosensitizers.

While these exploratory studies have demonstrated the potential of ZIFs in photocatalytic reactions, the roles that ZIFs play in these systems are either as inert hosts or remain blurred. Recently, our group found that ZIFs based on transition metal with unfilled d orbitals exhibit exceptional optical properties, including broad absorption bands in the UV-visible and near IR regions, with a surprisingly long-lived excited state for Co-ZIFs.[22] This suggests that ZIFs may afford facile charge separation (CS) and redox chemistry, desirable properties of heterogeneous photocatalysts. However, there have not yet been experimental reports of the CS dynamics from the excited state of ZIF materials. As fast and efficient charge transfer from excited ZIFs to substrates is essential for their application in photocatalysis, in this work, we report the first fundamental study of CS and charge recombination (CR) dynamics of ZIFs in the presence of methylene blue (MB$^+$) as an electron acceptor. Using ultrafast transient absorption (TA) spectroscopy, we observe the reduction of methylene blue by the ZIF-67 excited state following its selective excitation. This first insight into the CS dynamics of ZIF-67 will be essential toward developing ZIF materials as intrinsic light harvesting and CS materials for photocatalytic applications.

Experimental

Synthesis of ZIF-67 and MB$^+$-ZIF-67 films

ZIF-67 was prepared according to the published procedure.[22,23] 1.65 g of 2-methylimidazole (Alfa Aesar, Haverhill, Ma) and 0.73 g of Co(NO$_3$)$_2$·6H$_2$O (Acros Organics, Geel, Belgium) were each dissolved in 50 mL portions of methanol (Fisher Scientific, Fair Lawn, NJ). Quartz substrates (Ted Pella, Redding, CA) were treated with a piranha-etching solution (3 : 1 ratio of H$_2$SO$_4$: H$_2$O$_2$ by volume) overnight to functionalize the surface with

–OH groups for the facile attachment of ZIF-67. The etched substrates were rinsed with deionized water and placed in 20 mL glass vials for the ZIF-67 film growth. To the vial containing the film, 3 mL of $Co(NO_3)_2$ and 3 mL of 2-methylimidazole precursors were added quickly and the violet ZIF-67 solution was allowed 1 hour of growth time and then the film was removed from solution and rinsed with ethanol to represent a single ZIF-67 layer on the film. This process was repeated twice more to give a total of 3 ZIF-67 layers. Any ZIF-67 growth on the backside of the film was mechanically removed by wiping to give a ZIF-67 film on only one side of the substrate.

The ZIF-67 film was then sensitized with MB^+ (Acros Organics, Geel, Belgium) by soaking the ZIF-67 film in a 0.1 M methanol solution of MB^+ for 15 minutes. The film was then removed from solution and allowed to dry. The control sample, MB^+-quartz was synthesized by spin-coating a 0.1 M solution of MB^+ in methanol onto an etched quartz substrate until a comparable optical density to MB^+-ZIF-67 was obtained.

Table 1 TA kinetic fitting parameters with time constants τ and normalized amplitudes at selected representative wavelengths

Sample	Probe	τ_1, ps	A_1, %	τ_2, ps	A_2, %	τ_3, ps	A_3, %	τ_4	A_4, %
ZIF-67	508		41.6	—	—	—	—		58.4
	608		48.2[a]	—	—	—	—		51.8
	670	31.7	100	—	—	—	—	≫5 ns	—
MB^+-ZIF-67	580		41.9		26.4	101.4	1.3[a]		30.3
	608		42.1[a]	1.33	36.0[a]		14.0		7.9
	670		4.7		60.0		14.9[a]		20.4

[a]:Rising Component

Characterization

Steady-state UV-visible measurements were taken on a Cary 5000 UV-Vis-NIR spectrophotometer and reflective spectra were taken on the same spectrometer with an internal diffuse reflectance accessory. X-ray diffraction (XRD) was performed using a Rigaku Miniflex II XRD diffractometer with Cu Kα radiation. Since the film samples were too thin to perform reliable powder X-ray diffraction, the powdered ZIF-67 sample was obtained by centrifuging the post-film growth solution and collecting the precipitate. The precipitate was washed multiple times with methanol to remove the supernatant. MB^+-ZIF-67 for XRD characterization was prepared in a similar procedure as the film samples by soaking ZIF-67 powder in 0.1 M MB^+ solution for 15 minutes, centrifuging, and decanting the supernatant.

Transient optical absorption (TA) spectroscopy

TA spectroscopy was performed with a Helios ultrafast spectrometer (Ultrafast Systems LLC) with a regenerative amplified Ti-sapphire laser (Solstice, 800 nm, <100 fs fwhm, 3.5 mJ per pulse) at a 1 kHz repetition rate. The visible probe pulses are generated by white light generation in a sapphire window (430–800 nm). Pump pulses are generated in TOPAS, which generates tunable pump pulses from 235–1100 nm that are chopped at 500 Hz. The film sample was continuously translated to avoid sample damage and heating during the measurement. The excitation wavelength used in all TA experiments was 1000 nm with a power of 4.6 μJ per pulse.

Results and discussion

Thin films of ZIF-67 were prepared on a quartz substrate following our previously established procedure.[22] Three layers of ZIF-67 were grown consecutively to give an appropriately thick, transparent film for optical characterization. For the MB+ sensitized film (MB+-ZIF-67), the as-synthesized ZIF-67 was immersed in a 0.1 M solution of MB+ in methanol for 15 minutes, and was then removed from solution and allowed to dry. For a control sample (MB+-quartz), the MB+ solution was spin-coated onto a quartz substrate to give a transparent film of comparable optical density with respect to the MB+ on the MB+-ZIF-67 film.

The thin films were first characterized by diffuse reflectance UV-visible spectroscopy (Fig. 1a). The MB+-quartz sample (red spectrum) shows a prominent band from ~480–710 nm with an absorption tail into the near-IR region. The UV-visible band observed is much broader than that of the MB+ in solution (Fig. S1, ESI†). This phenomenon has been previously ascribed to dimerization, trimerization, or further aggregations of MB+ molecules resulting in significant broadening of the UV-visible features and the appearance of an absorption tail on the red-side of the peak.[24] In the spectra of the MB+-ZIF-67 film, a very similar MB+ peak profile is present, indicating that MB+-quartz is an appropriate control sample. Additional features characteristic of ZIF-67 were also observed in the spectra of MB+-ZIF-67. The prominent peak at 585 nm can be assigned to the higher-lying d–d transition of ZIF-67 ($[^4A_2(F)–^4T_1(P)]$) due to tetrahedral coordination of Co^{II} in the ZIF-67 structure.[22] The lower-lying $[^4A_2(F)–^4T_1(F)]$ d–d transition, which has a lower extinction coefficient than the higher-lying transition and much lower extinction coefficient than the MB+ features, is visible at the 900–1350 nm regime and is shown enlarged in Fig. S1 (ESI†). The higher-lying d–d transition in the spectrum of MB+-ZIF-67 does not shift with respect to that in bare ZIF-67 (inset, Fig. 1a), indicating that the bulk structure of ZIF-67 does not change due to MB+ adsorption. The unchanged structure of ZIF-67 in MB+-ZIF-67 was further confirmed by XRD in Fig. 1b, where the XRD patterns of MB+-ZIF-67 resemble that of ZIF-67 and are consistent with the published SOD-topology ZIF-67 patterns.[25]
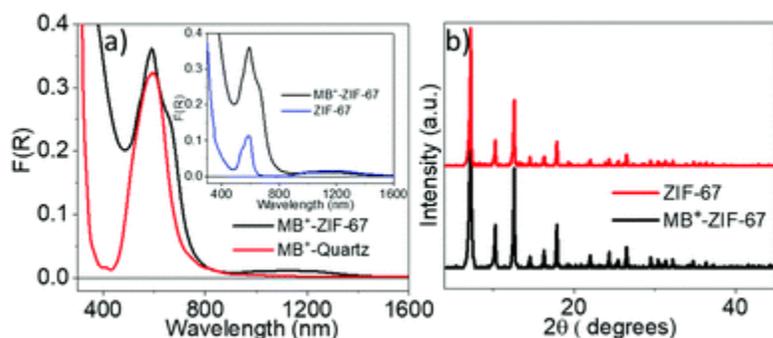

Fig. 1 (a) UV-visible reflectance diffuse spectra of MB+ on quartz and MB+ sensitized ZIF-67 films. Inset of (a) compares the UV-visible reflectance diffuse spectra of bare ZIF-67 and MB+ sensitized ZIF-67 films. (b) XRD patterns of bare ZIF-67 and MB+ sensitized ZIF-67 films.

The CS dynamics in MB+-ZIF-67 was investigated by femtosecond TA spectroscopy. Due to the significant spectral overlap of MB+ and ZIF-67 (Fig. 1a), we are not able to selectively excite MB+ or ZIF-67 in the visible spectral range. Instead, 1000 nm was used to selectively excite the lower-lying d–d transition of ZIF-67 as MB+ has negligible absorption at this wavelength. This was further confirmed by the TA spectra of the control sample, i.e. MB+-quartz, which yields a negligible TA signal under the same experimental conditions (Fig. S2, ESI†).

Fig. 2a shows the TA spectra of ZIF-67 following 1000 nm excitation. The instantaneously formed negative feature centered at 580 nm and broad positive features from 450 nm to 500 nm and 650 nm to 800 nm can be assigned to the ground state bleach (GSB) of ZIF-67 and the instantaneously formed excited Co d–d state (4T1) after photoexcitation that is intrinsic to ZIF-67, respectively. The Co d–d excited state features decay with time, which is accompanied by the formation of a prominent positive feature at 608 nm, corresponding to the formation of an intermediate long-lived charge separated state that is consistent with our previous observations on the ZIF-67 film.[22] However, distinct differences were observed in the spectra of MB^{+}-ZIF-67 (Fig. 2b) compared to that of ZIF-67. First, the GSB of ZIF-67 in the spectra of MB^{+}-ZIF-67 appears to decay faster while the growth of the positive feature at 608 nm is suppressed. Furthermore, an additional spectral feature, namely a broad negative feature, is visible from approximately 620 nm to 720 nm where it isn't overlapped by the larger ZIF-67 features. These features are highlighted in the inset of Fig. 2b, where the region from 600 nm to 750 nm in the MB^{+}-ZIF-67 transient spectra is enlarged. The new negative feature observed which extends to 720 nm, is consistent with the ground state absorption of MB^{+} and can thus be attributed to the GSB of MB^{+}. The formation of the GSB of MB^{+} in the spectra of MB^{+}-ZIF-67 can result from energy transfer or charge transfer processes from the excited ZIF-67 to MB^{+}. The energy transfer process from ZIF-67 to MB^{+} is not feasible in this system because of energy conservation; 1000 nm excitation is lower than the energy that can be absorbed by MB^{+}. We can also exclude the possibility of hole transfer from ZIF-67 to MB^{+} as this process is thermodynamically unfeasible (MB2^{+}/MB^{+} redox couple occurs at +1.105 V vs. SCE).[26,27] These results together lead us to believe that electron transfer occurs from excited ZIF-67 to MB^{+}, resulting in the formation of GSB of MB^{+}. We note that, while MB^{+} signals are clearly observed, the ET event must have limited efficiency since highly efficient ET would lead to dominating MB^{+}-centered features. This is likely due to the heterogeneous nature of the sample (i.e. dye aggregation) as well as the poor coupling between the electronic states of ZIF-67 and MB^{+} due to surface contact only and the aforementioned dye aggregation.
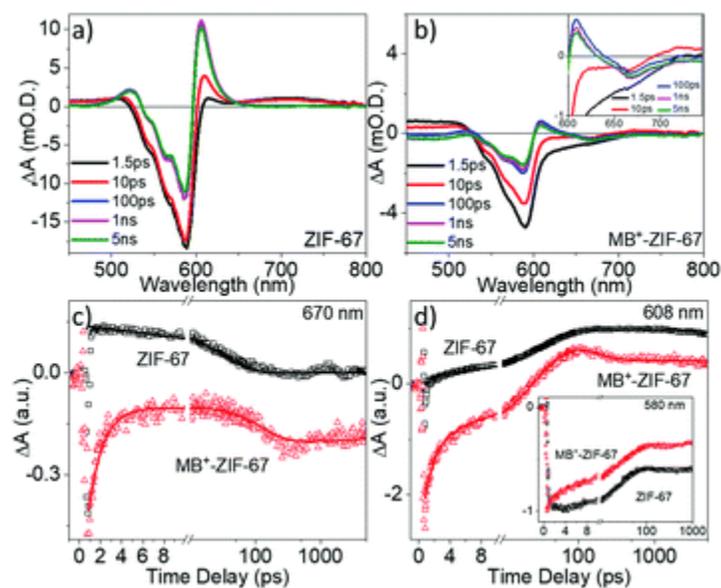

Fig. 2 Transient absorption spectra of (a) ZIF-67 and (b) MB^{+}-ZIF-67 following 1000 nm excitation. The comparison of TA kinetics of ZIF-67 and MB^{+}-ZIF-67 at 670 nm (c), 608 nm (d), and 580 nm (inset of d). Inset of (b) shows the enlarged MB^{+} GSB region. The solid lines in (c and d) are the best fit lines from the global multiexponential result.

Further evidence of the ET process can be seen from the TA kinetics of MB^{+}-ZIF-67. As shown in Fig. 2c and d, instead of positive amplitudes for the kinetics at 670 nm and 608 nm for ZIF-67, the kinetics of MB^{+}-ZIF-67 at

both wavelengths initiate with negative amplitudes, which suggests the instant formation of MB^+ GSB, accounting for an ultrafast ET process from the excited ZIF-67 to MB^+. The recovery of MB^+ GSB was observed at <10 ps, which can be attributed to the charge recombination (CR) process from reduced MB^+ and oxidized ZIF-67, consistent with the enhanced GSB recovery of ZIF-67 in MB^+-ZIF-67 (inset of Fig. 2d). Meanwhile, it is interesting to note that the GSB recovery of MB^+ stops after ~10 ps, which is indeed followed by the further growth of MB^+ GSB, as can be seen in the kinetic traces in Fig. 2c and d as well as the enlarged spectral region in the inset of Fig. 2b. We attributed this irregularity to ET from ZIF-67 to MB^+ but with a different pathway, the origin of which will be discussed in the next section. Different from the first ET pathway where the ultrafast CR process was observed, the CR associated with this second ET process is slow ($\gg$5 ns).

A multiexponential model was used to fit the kinetic traces at eight wavelengths globally across the TA probe range to quantify the kinetic trends observed (Table 1). The data <800 fs was excluded from the fits due to the combination of our 200 fs instrument response, coherent artifacts, and substrate effects that are visible in Fig. 2 as data points above and below the baselines of the kinetic traces at early times. To facilitate discussion, the kinetic traces at 580 nm, 608 nm, and 670 nm only are shown and compared here in the main text as they are representative of the assigned processes. The full global fit results are shown and discussed in the ESI† (Fig. S3 and Table S1). The ZIF-67 sample was first fit using the same time constant (τ_1 of 31.7 ps) found in our previous study at all wavelengths.[22] The 470 nm and 670 nm features, assigned to the decay of ZIF-67 ES, were completely recovered by 100 ps and, thus, were fit with a single exponential. The 580 nm and 608 nm features, however, included a $\gg$5 ns component to account for the remaining signal at the end of our TA time window of 5 ns. The fast decay at an early time of all kinetic traces was fit with τ_2 of 1.33 ps and is assigned to the recombination between some of the instantaneously generated $MB^·$ and ZIF-67+. The MB^+ GSB does not return to zero, however, indicating that some of the $MB^·$ persists beyond this first recombination component, possibly due to charge separation/delocalization. As mentioned previously, a distinct growth in all the kinetic features, except the ZIF-67 GSB feature at 580 nm where the remaining signal from ZIF-67 is relatively large, is present in the MB^+-ZIF-67 sample. To account for this signal growth, an additional time constant τ_2 of 101.4 ps needed to be included in the global fit model.

The evolution of TA features and the significant difference in time constants obtained can be well explained by a two-pathway model shown in Fig. 3a. Due to the periodic nature of the ZIF-67 framework, there are two classes of $[Co^{II}(mim)2]$ tetrahedron units: (1) the units that are located on the surface of the film and are directly in contact with MB^+ and (2) units that are in the bulk of the film and were isolated from MB^+ by the surface units. These different classes of $[Co^{II}(mim)2]$ tetrahedron units lead to distinctly different pathways for ET to MB^+ in the MB^+-ZIF-67 system, A and B, respectively (Fig. 3a). Pathway A is initiated by excitation of a ZIF-67 tetrahedron unit that is in direct contact or close proximity with MB^+, resulting in ultrafast ET to MB^+, followed by fast 1.33 ps recombination between $MB^·$ and ZIF-67+. Pathway B is initiated by excitation of a ZIF-67 tetrahedron unit that is not in direct contact with MB^+. Excitation results in the formation of an intermediate state (IMS) that we have previously shown to be an intrinsic charge-separated state in ZIF-67 with LMCT character.[22] We are unsure of the mechanism of charge separation within ZIF-67, which is an active area of research in our group, but it is suggested by our fundamental studies that it does occur and results in the long lifetime for photoexcited ZIF-67. The separated negative charge must then migrate to a site where it can reduce MB^+ from the long-lived IMS with a time constant of 101.4 ps. As evidenced by the lack of decay in the 670 nm kinetic trace (Fig. 2d) that can only be due to the GSB of $MB^·$ since ZIF-67 has no signal at this wavelength at later times, recombination does not occur within our time window.
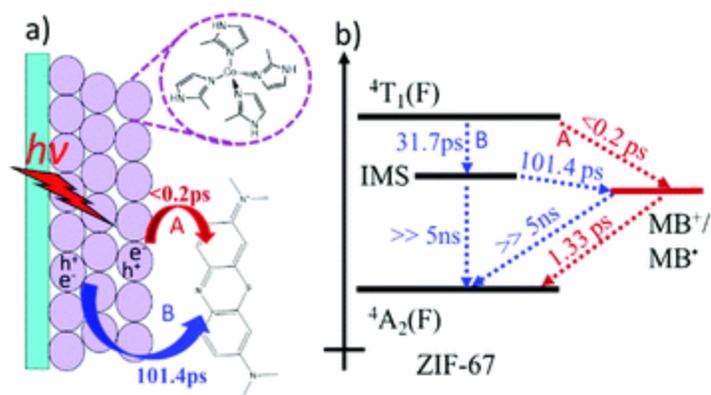
Fig. 3 (a) The proposed two-pathway electron transfer model in MB$^+$-ZIF-67. (b) Schematic diagram depicting energetics and time constants for electron transfer dynamics in MB$^+$-ZIF-67.

The scheme in Fig. 3b depicts the energetics diagram inferred from the above TA results. ZIF-67 is first excited with 1000 nm light to promote an electron from the Co-centered $^4A_2$(F) state to the Co-centered $^4T_1$(F) state. From this state, some ET occurs from the ZIF-67 $^4T_1$(F) state to MB$^+$ before our instrument response time (<200 fs) while the remaining excited state relaxes down to the IMS with a 31.7 ps time constant.[22] This 31.7 ps time constant should be unable to compete with the <200 fs component of ET. However, as we proposed in two-pathway model (Fig. 3a), there are ZIF-67 tetrahedron units that are not in contact with MB$^+$, which can prohibit the ultrafast ET event. In our previous study, the IMS has an amplitude weighted lifetime of 2.9 μs[22] and therefore does not evolve any further at a later time (>100 ps) of our TA time window. However, the additional rising component that fit with a time constant of 101.4 ps was observed and must be due to ET from the IMS state to MB$^+$, as the evolution of ZIF-67 features after the 31.7 ps component does not occur in the absence of MB$^+$. The two ET components are then associated with two recombination components of 1.33 ps and ≫5 ns, respectively.

While pathway A is important because it demonstrates the ability to extract an electron from ZIF-67 and provides a lower (positive) limit of −0.23 V vs. SCE for the position of the $^4T_1$(F) state electrochemical potential, the existence of pathway B is particularly interesting because it demonstrates the possibility to extract electrons from a super long-lived charge separated state intrinsic to ZIF-67. This characteristic is paramount to the successful application of photocatalytic materials, provided the electrochemical potential of the material is negative enough, on an electrochemical scale, to perform useful photocatalytic reactions. The following discussion will focus on recent examples in the literature that corroborate our findings here and demonstrate the applicability of ZIF materials to photocatalytic materials.

A computational study based on periodic structure calculations indicated that Zn-based ZIF analogues with various linkers and mixed linkers all have LUCO (lowest unoccupied crystal orbital) levels negative enough to perform important photocatalytic reactions such as the proton reduction reaction and the reduction of CO_2(g) to methane or methanol.[27] When Zn was replaced with Co, it was found that the Co 3d orbital was positioned significantly more negatively than the LUCO which could suggest that a charge-separated state with LMCT character in ZIF-67 would be capable of the redox activity observed in this study. A recent experimental work[18] demonstrated that a Co-based ZIF analogue with benzimidazole linkers, ZIF-9, can reduce CO_2(g) to CO(g) in conjunction with a molecular photosensitizer that reduces ZIF-9 to its anion, ZIF-9−. If a corollary is made to a reduced Co center from intrinsic CS after photoexcitation, then it is feasible that photoexcited Co^{II}-ZIF would have a similar redox potential to ZIF-9−. In unpublished experiments, we have verified the ability of ZIF-67 to perform CO_2 reduction to CO under the same conditions. On an electrochemical scale vs. SCE, CO_2 reduction

in aqueous media is reported to be −0.28 V, −0.158 V, and −0.005 V for the formation of the CO(g), CH$_3$OH(l) and CH$_4$(g) products, respectively.[28] These values compare well to the reported redox potential of MB$^+$ of −0.23 V vs. SCE, indicating that computational and experimental studies support our finding that ZIF-67 can reduce MB$^+$ after photoexcitation on an energetic basis.

Conclusions

In conclusion, we report that ZIF-67 can reduce MB$^+$ after photoexcitation. The dynamics of the ET event were characterized using ultrafast transient absorption spectroscopy after selective excitation of the ZIF-67 d–d transition, which demonstrated the formation of MB$^.$ on both an ultrafast (<200 fs) timescale and on a relatively longer (101.4 ps) timescale. The ultrafast time constant is likely the ET time from the tetrahedral units located on the surface of the film that are directly in contact with MB$^+$, while the 101.4 ps time constant is likely attributed to the ET time from the units in the bulk of the film that were isolated from MB$^+$ by the surface units. These results were compared with recent literature reports that corroborated the finding that the excited state redox potential of ZIF-67 is likely negative from the redox potential of MB$^+$, −0.23 V vs. SCE. Since we have found the study of ZIF-67 via electrochemical means to be inaccessible, it is exceedingly important to pinpoint the excited state redox potential of ZIF-67 via photophysical studies. This first direct evidence of Co^{II}-ZIF photoredox chemistry strongly imply that ZIFs have a large potential as intrinsic light harvesting and charge separation materials and deserve further attention to be developed as a viable and versatile photocatalyst material.

Conflicts of interest

There are no conflicts of interest to declare.

Acknowledgements

References

1. A. Phan , C. J. Doonan , F. J. Uribe-Romo , C. B. Knobler , M. O'Keeffe and O. M. Yaghi , *Acc. Chem. Res.*, 2010, **43** , 58 -67

2. B. R. Pimentel , A. Parulkar , E. K. Zhou , N. A. Brunelli and R. P. Lively , *ChemSusChem*, 2014, **7** , 3202 -3240

3. B. L. Chen , Z. X. Yang , Y. Q. Zhu and Y. D. Xia , *J. Mater. Chem. A*, 2014, **2** , 16811 -16831 .

4. K. S. Park , Z. Ni , A. P. Côté , J. Y. Choi , R. Huang , F. J. Uribe-Romo , H. K. Chae , M. O'Keeffe and O. M. Yaghi , *Proc. Natl. Acad. Sci. U. S. A.*, 2006, **103** , 10186 -10191

5. R. Banerjee , A. Phan , B. Wang , C. Knobler , H. Furukawa , M. O'Keeffe and O. M. Yaghi , *Science*, 2008, **319** , 939 -943

6. J. C. Tan , T. D. Bennett and A. K. Cheetham , *Proc. Natl. Acad. Sci. U. S. A.*, 2010, **107** , 9938 -9943

7. K. Eum , K. C. Jayachandrababu , F. Rashidi , K. Zhang , J. Leisen , S. Graham , R. P. Lively , R. R. Chance , D. S. Sholl , C. W. Jones and S. Nair , *J. Am. Chem. Soc.*, 2015, **137** , 4191 -4197

8. Y. Yang , W. Rodríguez-Córdoba and T. Lian , *J. Am. Chem. Soc.*, 2011, **133** , 9246 -9249

9. R. Li , X. Ren , X. Feng , X. Li , C. Hu and B. Wang , *Chem. Commun.*, 2014, **50** , 6894 -6897

10. A. Schejn , A. Aboulaich , L. Balan , V. Falk , J. Lalevee , G. Medjahdi , L. Aranda , K. Mozet and R. Schneider , *Catal. Sci. Technol.*, 2015, **5** , 1829 -1839

11. J. A. Thompson , C. R. Blad , N. A. Brunelli , M. E. Lydon , R. P. Lively , C. W. Jones and S. Nair , *Chem. Mater.*, 2012, **24** , 1930 -1936
12. K. C. Jayachandrababu , D. S. Sholl and S. Nair , *J. Am. Chem. Soc.*, 2017, **139** , 5906 -5915
13. L. T. L. Nguyen , K. K. A. Le and N. T. S. Phan , *Chin. J. Catal.*, 2012, **33** , 688 -696
14. L. T. L. Nguyen , K. K. A. Le , H. X. Truong and N. T. S. Phan , *Catal. Sci. Technol.*, 2012, **2** , 521 -528
15. L. Lin , T. Zhang , X. Zhang , H. Liu , K. L. Yeung and J. Qiu , *Ind. Eng. Chem. Res.*, 2014, **53** , 10906 -10913
16. H.-P. Jing , C.-C. Wang , Y.-W. Zhang , P. Wang and R. Li , *RSC Adv.*, 2014, **4** , 54454 -54462
17. T. T. Isimjan , H. Kazemian , S. Rohani and A. K. Ray , *J. Mater. Chem.*, 2010, **20** , 10241 -10245
18. S. Wang , W. Yao , J. Lin , Z. Ding and X. Wang , *Angew. Chem., Int. Ed.*, 2014, **53** , 1034 -1038
19. S. B. Wang and X. C. Wang , *Appl. Catal., B*, 2015, **162** , 494 -500
20. S. Yang , B. Pattengale , E. L. Kovrigin and J. Huang , *ACS Energy Lett.*, 2017, **2** , 75 -80
21. B. Pattengale , S. Yang , S. Lee and J. Huang , *ACS Catal.*, 2017, **7** , 8446 -8453
22. B. Pattengale , S. Yang , J. Ludwig , Z. Huang , X. Zhang and J. Huang , *J. Am. Chem. Soc.*, 2016, **138** , 8072 -8075
23. W. Xia , J. Zhu , W. Guo , L. An , D. Xia and R. Zou , *J. Mater. Chem. A*, 2014, **2** , 11606 -11613 D. Heger , J. Jirkovsk and P. Kln , *J. Phys. Chem. A*, 2005, **109** , 6702 -6709
24. J. Qian , F. Sun and L. Qin , *Mater. Lett.*, 2012, **82** , 220 -223
25. T. Takizawa , T. Watanabe and K. Honda , *J. Phys. Chem.*, 1978, **82** , 1391 -1396
26. R. Grau-Crespo , A. Aziz , A. W. Collins , R. Crespo-Otero , N. C. Hernández , L. M. Rodriguez-Albelo , A. R. Ruiz-Salvador , S. Calero and S. Hamad , *Angew. Chem., Int. Ed.*, 2016, **55** , 16012 -16016
27. J. L. White , M. F. Baruch , J. E. Pander , Y. Hu , I. C. Fortmeyer , J. E. Park , T. Zhang , K. Liao , J. Gu , Y. Yan , T. W. Shaw , E. Abelev and A. B. Bocarsly , *Chem. Rev.*, 2015, **115** , 12888 -12935

Footnotes

1. † Electronic supplementary information (ESI) available: UV-visible spectra of MB[+] in solution, MB[+]-quartz TA and kinetic fitting details. See DOI: 10.1039/c8cp02078g
2. ‡ Eisch Research Fellow during the academic year 2017–2018.